

Chandra detection of hotspot and knots of 3C 303

J. Kataoka¹, P. Edwards², M. Georganopoulos³, F. Takahara⁴, and S. Wagner⁵

¹ Tokyo Institute of Technology, Meguro-ku, Tokyo, Japan

² Institute of Space and Astronautical Science, Sagami-hara, Kanagawa, Japan

³ Laboratory for High Energy Astrophysics, NASA/GSFC, Greenbelt, MD, USA

⁴ Department of Earth and Space Science, Osaka University, Osaka, Japan

⁵ Landessternwarte Heidelberg, Königstuhl, Heidelberg, Germany

Received 17 October 2002 / Accepted 27 November 2002

Abstract. We report the detection at X-rays of the radio/optical hotspot and knots of 3C 303 from a short (15 ksec) *Chandra* exposure in 2001 March. The X-ray morphology is similar to that of the radio/optical emission with peaks in the X-ray emission found at 5.5'' (knot B), 9'' (knot C) and 17'' (hotspot) from the core of 3C 303. Despite the limited signal-to-noise ratio of the short *Chandra* exposure, the X-ray photon spectrum was measured for the hotspot. We construct the spectral energy distribution (SED) and find that the X-ray flux is well below the extrapolation of the radio-to-optical continuum, which we interpret as resulting from the production of X-rays via inverse Compton scattering of both synchrotron photons (SSC) and cosmic microwave background photons (EC/CMB). The magnetic field strength, region size, and the maximum energy of electrons are self-consistently determined for the hotspot to be $B \simeq 4.3 \mu\text{G}$, $R \simeq 6.5 \times 10^{21}$ cm, and $\gamma_{\text{max}} \simeq 1.4 \times 10^7$. This implies a magnetic field strength a factor of ~ 30 below the equipartition value; $B_{\text{eq}} \simeq 150 \mu\text{G}$. The origin of this large departure from equipartition is still uncertain, but the discrepancy is reduced if the plasma in the hotspot is moving with mildly relativistic speeds. Our observation of 3C 303, as well as recent *Chandra* detections of large scale jets and hotspots in a number of radio galaxies, confirm that particles are accelerated very efficiently in radio galaxies.

Key words. galaxies: active – galaxies: individual: 3C 303 – galaxies: jets – X-rays: galaxies

1. Introduction

It is generally believed that the vast bulk of cosmic-ray nuclei and electrons up to 10^{15} eV are accelerated in the shock waves of supernova remnants (SNR). There has been dramatic confirmation of this idea with the detection of three SNRs as sources of ~ 100 TeV particles, both in the X-ray and TeV γ -ray bands; SN 1006 (Koyama et al. 1995; Tanimori et al. 1998), RXJ 1713.7–3946 (Koyama et al. 1997; Muraishi et al. 2000; Enomoto et al. 2002) and Cassiopeia A (Hughes et al. 2000; Aharonian et al. 2001), although it is still a mystery why only three of more than 200 known SNRs are TeV γ -ray emitters. However, the cosmic ray spectrum extends well beyond 10^{15} eV, and so more powerful particle accelerators must exist in the universe. From the theory of Fermi acceleration, the maximum energy of electrons/ions is proportional to the system size R ; $E_{\text{max}} [\text{TeV}] \sim 10^3 R [\text{pc}] B [\mu\text{G}]$ (Hillas 1984). Thus the the location of strong shocks and more extended structures than SNRs can potentially accelerate particles above 100 TeV. The large scale jets and lobes in extragalactic sources are good candidates for such acceleration sites (e.g., Hillas 1984; Gaisser 2000).

Jets are commonly observed in the radio galaxies, representing outflows that are well collimated on scales of tens to

hundreds of kiloparsecs (kpc). In spite of a long history of study, however, the processes by which the jets are formed and collimated are still far from being understood. Detailed spatial imaging can potentially trace the energy transport from the vicinity of the central black hole to the outer jet region, but observations with high spatial resolution ($\leq 1''$) have until recently only been possible at radio and optical wavelengths. Observations of jets at shorter wavelengths are extremely important because they can probe the sites of higher energy particle acceleration. Until the advent of *Chandra*, nonthermal X-ray emission had been detected from only a few kpc-scale jets by *Einstein* and *ROSAT* (e.g., Biretta et al. 1991; Röser et al. 2000). Marginal X-ray detections were reported also for the hotspots in which the jets are believed to terminate (Harris et al. 1994; Harris et al. 1998).

The *Chandra* X-ray Observatory has now resolved the X-ray spatial structure along jets, from kpc to Mpc, of more than a dozen of radio galaxies and quasars; e.g., PKS 0637–752 (Schwartz et al. 2000; Chartas et al. 2000), M 87 (Marshall et al. 2002; Wilson & Yang 2002), 3C 273 (Sambruna et al. 2001), and Cen A (Kraft et al. 2002). These observations have established that X-ray emission from large scale jets is more common than had been expected. X-rays have also been detected clearly from a number of lobes and hotspots (e.g., Wilson 2000; Wilson 2001 for Pictor A and Cygnus A; see Hardcastle et al. 2002 for a review). X-ray observations of

nonthermal emission from hotspots are of particular interest to constrain the energetics and the spectrum of the relativistic electrons. For example, the presence of high energy electrons with very short radiative life-times provides direct evidence for re-acceleration in the hotspot.

3C 303 ($z = 0.141$) is an unusual double radio source with a highly asymmetrical structure. This source is classified as a broad-line radio galaxy and had been thought to be a strong X-ray “point source”. In the *ROSAT* HRI image a faint point-like component, containing 25 ± 6 counts, was found approximately coincident with the western hotspot of 3C 303 (Hardcastle & Worrall 1999). However photon statistics and image resolution were not sufficient to confirm that the X-ray detection was associated with the hotspot. In particular, it was not possible to rule out a background ($z = 1.57$) QSO as the source of the X-rays (see below). In this letter, we report on the *Chandra* discovery of X-ray emission from the hotspot and knots of 3C 303. By combining the data from radio to X-rays, we show that radio galaxies accelerate particles to energies of 10–100 TeV in the hotspot. Throughout this paper, we adopt $H_0 = 75 \text{ km s}^{-1} \text{ Mpc}^{-1}$ and $q_0 = 0.5$, so $1''$ corresponds to 2.1 kpc at the redshift of 3C 303.

2. Observation and data analysis

2.1. Radio, infrared, and optical observations

The western hotspot of 3C 303 has been well studied at radio wavelengths. A 1.5 GHz VLA image of 3C 303 is shown in Fig. 1a (Leahy & Perley 1991). A prominent one-sided jet leads to a complex radio hotspot (Lonsdale et al. 1983) located at a projected distance of $17''$ (36 kpc) from the nucleus. The hotspot is actually double (components A_1 and A_2 in the 408 MHz map of Lonsdale et al. 1983), with the southern spot (A_2) being the brighter in radio images. Also, three faint jet components (knots A, B, C in Fig. 1a) are linearly spaced between the nucleus and the hotspot. The 1.5 GHz image of Leahy and Perley (1991), made with the VLA in A and B configurations, provided the first detection of the fainter hotspot on the eastern side of the core. The fact that the eastern lobe is significantly less polarized than the western lobe was ascribed to the Laing-Garrington effect (Laing 1988; Garrington et al. 1988), confirming that the jet on the western side is directed towards us, and that the counter-jet is on the eastern side.

Recently, Giovannini et al. (2001) derived limits for the angle to the line of sight, jet speed and Doppler factor of 24 radio galaxies based on the jet-to-counter-jet ratio and core dominance. For 3C 303, they derived a Doppler beaming factor in the range $0.80 \leq \delta \leq 1.79$ by assuming a bulk Lorentz factor of $\Gamma_{\text{BLK}} = 5$. They presented a single epoch 5 GHz VLBI image which shows a number of parsec-scale jet components (Fig. 15 in Giovannini et al. 2001), however, as no other VLBI images have been published, it is not yet possible to determine the apparent jet speed directly.

An infrared image of 3C 303 is presented in Fig. 1g of Meisenheimer et al. (1997). They detected a clear signal from the hotspot (A_2) and the jet which connects the nucleus with the hotspot. The background QSO, $21''$ from the nucleus and

to south-west of the hotspot, identified by Kronberg (1976) was also detected.

An optical counterpart of the multiple radio hotspot was found by Lelièvre & Wlérick (1975) and Kronberg (1976). Higher resolution images were obtained by Lähteenmäki & Valtaoja (1999) using the 2.5-m Nordic Optical Telescope on La Palma in 1992 June. They showed that the total extent of the hotspot, as measured from the outermost 3σ contours, is $2.3'' \times 3.1''$, corresponding to a linear size of 4.9–6.6 kpc (without correction of the broadening effect of the optical PSF and the seeing of 0.6–0.8"). The optical emission from the fainter northern hotspot (A_1) was not detected, indicating that radio-optical spectral indices are different in the two components. Considering the non-stellar structure of the image, the positional agreement, and the optical polarization, they argue that the optical candidate is a genuine counterpart to the radio hotspot (A_2) of 3C 303.

2.2. X-ray observations

Chandra observed 3C 303 on 2001 March 23 in a guaranteed time observation. The source was at the nominal aimpoint of the Advanced CCD Imaging Spectrometer S3 chip (ACIS-S3), and the exposure was continuous for 15.10 ksec. We have analyzed archival data on 3C 303 provided by HEASARC Browse (<http://heasarc.gsfc.nasa.gov/dp-per1/W3Browse/Browse.pl>). The raw level-1 data were reprocessed using the latest version (CIAO 2.1) of the CXCDs software. We generated a clean data set by selecting the standard grades (0, 2, 3, 4 and 6) and energy band 0.4–8 keV.

The X-ray image, produced by smoothing the raw *Chandra* image with a Gaussian of width $0.5''$ in the energy range of 0.4–8 keV, is shown in Fig. 1b. X-ray emission can be clearly seen from the bright central core, the western jet knots, and the hotspot (A_2). The total extent of the X-ray hotspot (A_2), measured from the outermost of 3σ contours in raw(un-smoothed) image, was $\sim 2.5''$. This is consistent with the optical extent of the hotspot, though we do not take into account the broadening of *Chandra* PSF ($\sim 0.5''$ half-energy radius, but with significant “wings” at larger scales). There is a suggestion of faint X-ray emission from the northern hotspot A_1 , but due to limited photon statistics no conclusive statement can be made. No emission was detected exceeding the background level at the location of the weak eastern hotspot seen in Fig. 15 of Leahy & Perley (1991).

The object just to the south-west of the hotspot is the background QSO at $z = 1.57$ mentioned previously (72 counts; 8.5σ). Knots B and C are marginally detected at the 4.5σ (20 counts) and 4.4σ (19 counts) levels, respectively. The innermost knot (A in Fig. 1a) cannot be resolved due to the contamination from the bright nucleus.

The nucleus is a very bright point source, with the $>30\%$ photon pile-up preventing us from performing any meaningful spectral or spatial analysis of this region. As an alternative, we have analyzed archival *ASCA* data to determine the X-ray flux and the spectral shape of the nuclear emission. *ASCA* observed 3C 303 in 1995 May and 1996 January, with a

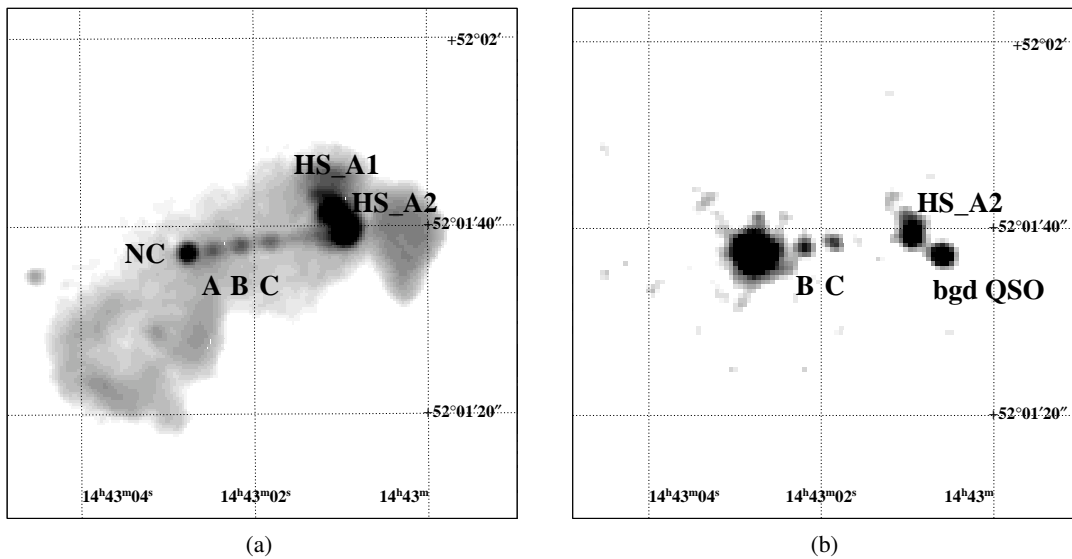


Fig. 1. **a)** Radio image of 3C 303. The grey scale is a 1.5 GHz VLA image (Leahy & Perley 1991; actually taken from Leahy et al. 1998). The resolution is 1.2 arcsec and black represents 20 mJy beam^{-1} . NC denotes the nucleus; A, B and C the jet knots; and HS_A1 and HS_A2 the hotspot components. **b)** X-ray image of 3C 303 in the 0.4–8 keV band (ACIS-S onboard *Chandra*). The image is smoothed with a $\sigma = 0.5$ arcsec Gaussian. B and C denotes the jet knots, and HS_A2 the hotspot component A₂.

20 ksec exposure each time. The X-ray fluxes were $2.6 \times 10^{-12} \text{ erg cm}^{-2} \text{ s}^{-1}$ in both observations (Table 1). No significant variation in the flux was detected between the two observations. Note that, due to the image resolution of $\sim 3'$, the jet, hotspot, and background QSO cannot be separated from the nucleus for the *ASCA* data, however, as indicated in Table 1, the contribution of these components to the nuclear flux is expected to be only $\sim 2\%$. Also, the nuclear flux may have been changed between *ASCA* and *Chandra* epochs. Despite these uncertainties, the flux measured with *ASCA* is consistent with that expected from the piled-up fraction observed with *Chandra*.

In order to minimize the contamination from neighboring regions for spectral fitting, we extracted the X-ray emission from the hotspot (A₂), knots B and C, and the background QSO, with circular regions of $3.0''$, $1.5''$, $1.5''$, and $1.5''$ radius, respectively. Approximately 95% of counts are collected with a circular region of $1.5''$ radius for a point source. Background subtractions were performed for each region, where the background counts were accumulated at the same off-nuclear distance to the component regions.

The fitted spectra are summarized in Table 1. Errors quoted in the table correspond to 1σ uncertainties for the parameter, unless otherwise stated. In each case, we assumed a power-law function absorbed by Galactic N_{H} only (fixed to $1.6 \times 10^{20} \text{ cm}^{-2}$; Stark et al. 1992). The hotspot and the background QSO were adequately fitted with this model. The X-ray photon index was $\Gamma_{\text{HS}} = 1.4 \pm 0.2$, and the corresponding 2–10 keV flux was $3.7 \times 10^{-14} \text{ erg cm}^{-2} \text{ s}^{-1}$ for the hotspot. Due to the limited photon statistics, we cannot determine the spectra shape for knots B and C. We thus fixed the spectral index to $\Gamma_{\text{knot-B,C}} = 2.0$ and estimated the flux. The X-ray fluxes of the knots B and C were $3.5 \times 10^{-15} \text{ erg cm}^{-2} \text{ s}^{-1}$ and $3.5 \times 10^{-15} \text{ erg cm}^{-2} \text{ s}^{-1}$ in 2–10 keV band, respectively.

For the background QSO, $\Gamma_{\text{QSO}} = 2.0 \pm 0.3$, and the corresponding 2–10 keV flux was $1.6 \times 10^{-14} \text{ erg cm}^{-2} \text{ s}^{-1}$. We remark again that although we have taken great care in reducing the data, it is impossible to eliminate the contamination of bright nucleus completely for knots B and C. Thus we mainly consider the hotspot (A₂) in the following as it was detected at high significance (92 counts; 9.6σ level) and is well separated from the nucleus ($17''$).

3. Discussion and conclusion

Using a short (15 ksec) *Chandra* observation, we have detected the X-ray counterpart of the radio-optical hotspot (A₂) and knots B and C in the radio galaxy 3C 303. Figure 2 shows the SEDs from radio to X-ray energies of the western hotspot (A₂). The radio-to-optical data are taken from Meisenheimer et al. (1997). This clearly indicates that the X-ray flux obtained with *Chandra* is well below the extrapolation from the radio-to-optical continuum. While the radio-to-optical continuum is generally believed to be synchrotron radiation, the radiative mechanisms usually considered as the possible origin of X-rays are either synchrotron (e.g., Pesce et al. 2001; Marshall et al. 2002) or inverse Compton scattering on various possible sources of soft photons including the synchrotron photons (SSC; e.g., Hardcastle et al. 2002) and the cosmic microwave background (EC/CMB; e.g., Tavecchio et al. 2000; Sambruna et al. 2001).

Relativistic boosting appears to be necessary to explain the X-ray jet emission in the detected core-dominated radio-loud quasars. Depending on the assumptions of jet Doppler factor, different authors have reached different conclusions for the physical processes to account for the SEDs (compare, e.g., Schwartz et al. 2000 with Tavecchio et al. 2000). However, the

Table 1. Spectral fits to the 3C 303 knots, hotspot, and the background QSO.

region	image radius ^a	photon index ^b	2–10 keV flux ^c	red. χ^2 (dof)
hotspot (A ₂)	3.0	1.4 ± 0.2	$(3.7 \pm 0.5) \times 10^{-14}$	0.43(7)
knot B	1.5	2.0(fixed)	$(3.5 \pm 1.2) \times 10^{-15}$	0.19(2)
knot C	1.5	2.0(fixed)	$(3.5 \pm 1.2) \times 10^{-15}$	1.2(1)
QSO	1.5	2.0 ± 0.3	$(1.6 \pm 0.3) \times 10^{-14}$	0.74(6)
nucleus ^d	180	1.65 ± 0.05	$(2.6 \pm 0.2) \times 10^{-12}$	0.8(29)
nucleus ^e	180	1.60 ± 0.08	$(2.6 \pm 0.3) \times 10^{-12}$	0.6(13)

^a Radius (in arcsec) of a circular region to extract X-ray counts.

^b The best fit power-law photon index assuming a Galactic N_H of 1.6×10^{20} cm⁻².

^c In unit of erg cm⁻² s⁻¹.

^d Analysis of archival *ASCA* data (1995 May).

^e Analysis of archival *ASCA* data (1996 January).

role of Doppler boosting in the case of hotspots is still unclear. Since hotspots are where the jet is thought to be terminated, it is natural to consider that jet plasma is not beamed, or is only mildly beamed. Furthermore, a statistical analysis of samples of FR II radio galaxies implies non-relativistic velocities in the hotspots (e.g., Arshakian & Longair 2000). Taking the results of Giovannini et al. (2001) into account, we start from the assumption of a Doppler beaming factor of $\delta = 1$.

Assuming a spherical geometry for the emission region, the radius of the hotspot (A₂) is set to $R \sim 6.5 \times 10^{21}$ cm ($\sim 1''$; see Sect. 2) from the radio, optical, and X-ray images. By fixing R and δ , other physical parameters and the electron population are tightly constrained. As described in the literature (e.g., Kino et al. 2002; Kataoka et al. 2002), jet parameters are closely connected with the observed quantities. The synchrotron cut-off frequency, ν_{\max} , is given by

$$\nu_{\max} \simeq 1.2 \times 10^6 B \gamma_{\max}^2 (1+z)^{-1} \text{ Hz}, \quad (1)$$

where B is the magnetic field strength and $\gamma_{\max} m_e c^2$ is the maximum electron energy. Although the position of the synchrotron cut off is quite uncertain, we infer that it must be between optical and X-ray energy bands; $10^{14} \text{ Hz} \leq \nu_{\max} \leq 10^{16} \text{ Hz}$. This leads to a condition in the B – γ_{\max} plane,

$$9.5 \times 10^7 \leq B \gamma_{\max}^2 \leq 9.5 \times 10^9. \quad (2)$$

The synchrotron luminosity is given by

$$L_{\text{sync}} = 4\pi R^2 c U_{\text{sync}}, \quad (3)$$

where R is the radius of the emission region, which we have set to $R = 6.5 \times 10^{21}$ cm. We calculate the synchrotron luminosity integrated over all frequencies using the formula given by Band & Grindlay (1985). Assuming an electron population of the form $N(\gamma) = N_0 \gamma^{-s} \exp(-\gamma/\gamma_{\max})$, where with the electron power law index set to $s = 2.7$ from the radio spectral index $\alpha \simeq 0.84$ (Meisenheimer et al. 1997), we obtain $L_{\text{sync}} = 1.2 \times 10^{43}$ erg s⁻¹. Thus the synchrotron photon density is given as $U_{\text{sync}} = 1.7 \times 10^{-12}$ erg cm⁻³. Comparing this with the cosmic microwave background (CMB) photon energy density, $U_{\text{CMB}} = 4.1 \times 10^{-13} (1+z)^4 = 6.9 \times 10^{-13}$ erg cm⁻³, the synchrotron photon density is about a factor of two larger. This

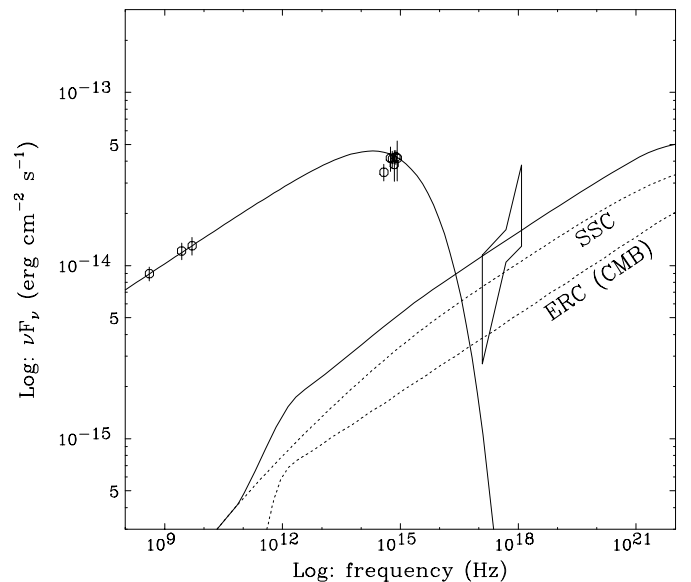


Fig. 2. SED of hotspot (A₂) of 3C 303 (see Fig. 1). The radio to optical data comes from Meisenheimer, Yates and Röser 1997. The *bow tie* shows the X-ray data from *Chandra* observation (this work; 90% error in 0.5–5 keV). The solid line represents a fit assuming synchrotron emission for the radio to optical range and inverse Compton scattering of synchrotron (SSC) plus CMB photons (EC/CMB) for the X-ray emission, and yields $R = 6.5 \times 10^{21}$ cm, $B = 4.3 \mu\text{G}$ and $\gamma_{\max} = 1.4 \times 10^7$. Uncertainties in the physical parameters are discussed in the text and Fig. 3.

indicates that the dominant source of seed photons which are upscattered to the X-rays is synchrotron photons, but that CMB photons are of comparable importance.

The ratio of the synchrotron luminosity to the SSC and EC/CMB luminosities is given by

$$\frac{L_{\text{SSC}} + L_{\text{EC/CMB}}}{L_{\text{sync}}} = \frac{U_{\text{sync}} + U_{\text{CMB}}}{U_B}, \quad (4)$$

where U_B is the magnetic field density ($U_B = B^2/8\pi$). Due to lack of γ -ray observations, we cannot measure Compton luminosity ($L_{\text{SSC}} + L_{\text{EC/CMB}}$) accurately, however, it must be larger than the “X-ray luminosity” which is defined in the *Chandra* bandpass ($L_X \equiv 4\pi d_L^2 f_X = 9.2 \times 10^{41}$ erg s⁻¹, where d_L

is the luminosity distance to 3C 303 and f_X is the 0.4–8 keV flux). This is because (i) the X-ray spectrum is still “rising” in the νF_ν plane (see Fig. 2) and (ii) the X-ray flux consider only a small part (0.4–8 keV) of overall inverse Compton emission. Considering this inequality, $L_{\text{SSC}} + L_{\text{EC/CMB}} \geq L_X$, the magnetic field is estimated as

$$B \leq 28 \mu\text{G}. \quad (5)$$

Combining Eqs. (2) and (5), the “allowed” region of the B – γ_{max} plane is shown as the hatched region in Fig. 3. The input parameters for our model are those at the center of this region, and the resultant fit is given as solid line in Fig. 2. We assume an electron population of a form $N(\gamma) = N_0 \gamma^{-s} \exp(-\gamma/\gamma_{\text{max}})$, where $N_0 = 0.9 \text{ cm}^{-3}$, $\gamma_{\text{max}} = 1.4 \times 10^7$, and $s = 2.7$. We set the minimum Lorentz factor of electrons (γ_{min}) to 1, and the magnetic field to $B = 4.3 \mu\text{G}$, respectively. Note that parameters we have chosen are valid even if the actual Compton luminosity is an order of magnitude larger, in which case Eq. (5) would be $B \leq 8.9 \mu\text{G}$.

In Fig. 3, we also show the region typical for “blazars” for comparison (adapted from Ghisellini et al. 1998; Kubo et al. 1998). Blazars are characterized by strong jet emission and the radiation is thought to be emitted from a relativistic jet directed close to our line of sight (e.g., Urry & Padovani 1995). More than 70 blazars are strong GeV and/or TeV γ -ray emitters, indicating that particles are accelerated very efficiently in sub-pc scale jets up to $\gamma_{\text{max}} \sim 10^6$ (e.g., Ghisellini et al. 1998; Kubo et al. 1998). Interestingly, our current analysis of 3C 303 implies that the hotspots of radio galaxies may be *more* powerful particle accelerators than blazars, with particles being accelerated up to 10–100 TeV.

Recent *Chandra* and *ROSAT* detections of large scale jets and hotspots provide additional evidence for extremely relativistic particles in a number of radio galaxies: M 87 (Wilson & Yang 2002: $\gamma_{\text{max}} \sim 10^{7-8}$), 3C 390.3 (Harris et al. 1998: $\gamma_{\text{max}} \sim 7.5 \times 10^7$), and 3C 371 (Pesce et al. 2001: $\gamma_{\text{max}} \sim 4 \times 10^7$). Similar characteristics, such as steep spectral indices and high-frequency cutoffs, have also been reported for a number of hotspots in other sources (3C 123, Pictor A, 3C 295, 3C 351; see Harris & Krawczynski 2002). Although the sample size is still small, it appears that large scale jets/hotspots in radio galaxies are an important acceleration site in the universe.

If the electrons are actually accelerated to such high energies, the electrons emitting via synchrotron in the optical band and via inverse Compton at γ -ray energies have relatively short lifetimes. The cooling time of electrons is

$$t_{\text{cool}}(\gamma) = \frac{3m_e c}{4(U_B + U_{\text{sync}} + U_{\text{CMB}})\sigma_T \gamma}. \quad (6)$$

Assuming the parameters used to model the SED, $\gamma_{\text{max}} = 1.4 \times 10^7$ and $B = 4.3 \mu\text{G}$, we obtain $t_{\text{cool}}(\gamma_{\text{max}}) = 7.0 \times 10^{11} \text{ s}$. In other words, the highest energy electrons can travel $d \sim ct_{\text{cool}} = 6.8 \text{ kpc}$ before losing their energy. This is consistent with the size of the hotspot, but smaller than the projected distance from the nucleus (36 kpc), implying the electrons can originate from a single acceleration site in the hotspot. However considering the uncertainties in the B – γ_{max}

plane, we cannot establish with this data alone that electrons entering in the hotspot actually need to be re-accelerated.

One difficulty of understanding the overall photon spectrum with the above simple picture is that the relativistic electron energy density significantly exceeds the magnetic field density ($U_e \gg U_B$). For the parameters used to fit the SED (Fig. 2), we expect $U_e/U_B \simeq 1.4 \times 10^6 \gamma_{\text{min}}^{-0.7}$, where γ_{min} is the minimum Lorentz factor of electrons. An equipartition magnetic field $B_{\text{eq}} \sim 150 \mu\text{G}$ ($B_{\text{eq}}/B \geq 30$), underproduces the X-ray flux. Such large departures from equipartition have been suggested for other X-ray hotspot sources, namely Pictor A ($B_{\text{eq}}/B \simeq 14$; Wilson et al. 2001) and 3C 351 ($B_{\text{eq}}/B \simeq 12$ for the northern hotspot, and <25 for the southern hotspot; Hardcastle et al. 2002).

The process responsible for the anomalously bright, flat X-ray hotspots in these sources is still an open question. Hardcastle et al. (2002) have suggested a number of possibilities, some of which may also be applicable for 3C 303 hotspots. One idea is that the hotspot is mildly beamed rather than stationary. Beaming causes the observed flux densities to change by a factor $\delta^{3+\alpha}$ (Dermer & Schlickeiser 1993), where δ is the Doppler beaming factor. For an electron population with energy index s , the predicted SSC flux scales as $\delta^{-12/(s+5)} \simeq \delta^{-1.6}$, and so Doppler dimming ($\delta < 1$) increases the predicted equipartition flux. To place 3C 303 at equipartition with the beamed SSC emission, we thus require $\delta \sim 0.01$. This strongly conflicts with the range derived from radio observations, $0.80 \leq \delta \leq 1.79$ (Giovannini et al. 2001), although these limits were based in part on the properties of the parsec-scale jet, and thus it may be possible that the downstream hotspot has quite a different Doppler factor.

For the case of 3C 303 hotspot, however, considering the SSC emission alone is not sufficient because the synchrotron photon energy density only marginally dominates over the CMB photon energy density (by about a factor of two; see above). For a source in equipartition the normalization factor of the electron number density scales as $N_0 \propto L_s B_{\text{eq}}^{-(1+\alpha)}$ (Longair 1994), where L_s is the synchrotron comoving luminosity at a fixed frequency for a source of a given comoving volume. The equipartition magnetic field is $B_{\text{eq}} \propto L_s^{2/7}$. Combining these two equations, we obtain $N_0 \propto L_s^{(5-2\alpha)/7}$. The observed synchrotron luminosity at the same fixed frequency is $L_{\text{obs}} = L_s \delta^{3+\alpha}$. Using this, we obtain $N_0 \propto \delta^{-(3+\alpha)(5-2\alpha)/7}$. Therefore, for a given observed synchrotron spectrum, as the beaming increases, the electron number density in equipartition decreases. The external Compton emission is $L_{\text{EC}} \propto N_0 \delta^{4+2\alpha}$ (Dermer 1995; Georganopoulos et al. 2001). Substituting N_0 we obtain $L_{\text{EC}} \propto \delta^{(2\alpha^2+15\alpha+13)/7}$. Therefore, although the electron number density decreases as δ increases, the external Compton emission increases. Setting $\alpha = 0.84$, for a hotspot Lorentz factor $\Gamma_{\text{BLK}} = 2$ at an angle $\theta = 30^\circ$ the external Compton emission is boosted by a factor of ~ 15 . Such hotspot Lorentz factors are routinely observed in hydrodynamic simulations (e.g., Aloy et al. 1999).

In conclusion, we suggest that for typical orientation angles of $\sim 30^\circ$, the hotspot of 3C 303 would be closer to equipartition if it were mildly beamed, but it is not clear if beaming alone

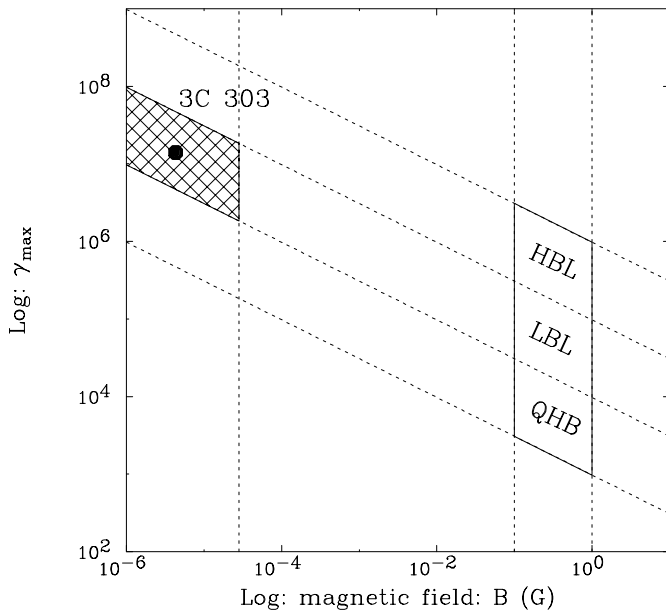


Fig. 3. The parameter space (B , γ_{\max}) allowed by the one-zone synchrotron plus SSC+EC/CMB model for the 3C 303 hotspot. Filled circle represents parameters which fit the SED (see Fig. 2). The allowed parameter space for sub-pc scale jets in blazars are shown for comparison. HBL, High Frequency Peaked BL Lac; LBL, Low Frequency Peaked BL Lac; and QHB, QSO hosted blazars (adapted from Kubo et al. 1998 and Ghisellini et al. 1998).

can account for the large departure from equipartition. Many theoretical models are now being developed, involving the hydrodynamic simulations and MHD calculations, to understand the physical conditions in hotspots (Aloy et al. 1999; Tregillis et al. 2001; Saxton et al. 2002). These numerical simulations lead us to expect that hotspots are transient structures, and may well have different magnetic field and electrons acceleration behaviour at different times. If this is the case, it might be possible that the hotspots are being in a temporary transition state, far from equipartition.

We finally comment on the X-ray emissions from knots B and C, which may be compared to the hotspot(A_2) emission. Our preliminary analysis shows that the radio flux of knots B and C at 1.5 GHz is $\sim 6 \times 10^{-16}$ erg cm $^{-2}$ s $^{-1}$, which is about five times fainter than the corresponding X-ray fluxes (Table 1). The flux ratio between the radio and X-ray bands is almost equal to that of the hotspots A_2 ($f_X/f_{\text{radio}} \simeq 4$). This may imply that the SED of knots B and C could be similar to that of the hotspot, although the knots are a priori more likely to be moving at relativistic speeds than hotspot A_2 . Unfortunately, optical detections of knots B and C have not yet been reported and so we cannot confirm this suggestion at present. Deeper *Chandra* and *HST* observations of radio galaxies will allow us to understand the kinematics of the jet knots hotspot and further study their likely role as one of the most efficient particle accelerators in the universe.

Acknowledgements. We deeply appreciate the insightful comments and suggestions of the referee, M.J. Hardcastle, that have improved this paper considerably. J.K. acknowledges a Fellowship of the Japan Society for Promotion of Science for Japanese Young Scientists.

References

- Aharonian, F., Akhperjanian, A., Barrio, J., et al. 2001, *A&A*, 370, 112
- Aloy, M. A., Ibanez, J. M., Marti, J. M., Gomez, J.-L., & Muller, E. 1999, *ApJ*, 523, L125
- Arshakian, T. G., & Longair, M. S. 2000, *MNRAS*, 311, 846
- Band, D. L., & Grindlay, J. E. 1985, *ApJ*, 298, 128
- Biretta, J. A., Stern, C. P., & Harris, D. E. 1991, *AJ*, 101, 1632
- Chartas, G., Worrall, D. M., Birkinshaw, M., et al. 2000, *ApJ*, 542, 655
- Dermer, C. D. 1995, *ApJ*, 446, L63
- Enomoto, R., Tanimori, T., Naito, T., et al. 2002, *Nature*, 416, 823
- Gaisser, T. K. 2000, in *High Energy Gamma-ray Astronomy*, ed. F. A. Aharonian, & H. J. Völk, *AIP Conf. Ser.*, 558, 27
- Garrington, S. T., Leahy, J. P., Conway, R. G., & Laing, R. A. 1988, *Nat*, 331, 147
- Georganopoulos, M., Kirk, J. G., & Mastichiadis, A. 2001, *ApJ*, 561, 111
- Ghisellini, G., Celotti, A., Fossati, G., Maraschi, L., & Comastri, A. 1998, *MNRAS*, 301, 451
- Giovannini, G., Cotton, W. D., Feretti, L., Lala, L., & Venturi, T. 2001, *ApJ*, 552, 508
- Hardcastle, M. J., & Worrall, D. M. 1999, *MNRAS*, 309, 969
- Hardcastle, M. J., Birkinshaw, M., Cameron, R. A., et al. 2002, *ApJ*, in press [astro-ph/0208204]
- Harris, D. E., Carilli, C. L., & Perley, R. A. 1994, *Nature*, 367, 713
- Harris, D. E., Leighly, K. M., & Leahy, J. P. 1998, *ApJ*, 499, L149
- Harris, D. E., & Krawczynski, H. 2002, *ApJ*, 565, 244
- Hillas, A. M. 1984, *ARA&A*, 22, 425
- Hughes, J. P., Rakowski, C. E., Burrows, D. N., & Slane, P. O. 2000, *ApJ*, 528, L109
- Kataoka, J., Tanihata, C., Kawai, N., et al. 2002, *MNRAS*, 336, 932
- Kino, M., Takahara, F., & Kusunose, M. 2002, *ApJ*, 564, 97
- Koyama, K., Petre, R., Gotthelf, E. V., et al. 1995, *Nature*, 378, 255
- Koyama, K., Kinugasa, K., Matsuzaki, K., et al. 1997, *PASJ*, 49, L7
- Kraft, R. P., Forman, W. R., Jones, C., et al. 2002, *ApJ*, 569, 54
- Kronberg, P. P. 1976, *ApJ*, 203, L47
- Kubo, H., Takahashi, T., Madejski, G., et al. 1998, *ApJ*, 504, 693
- Lähteenmäki, A., & Valtaoja, E. 1999, *ApJ*, 117, 1168
- Laing, R. A. 1988, *Nature*, 331, 149
- Leahy, J. P., & Perley, R. A. 1991, *AJ*, 102, 537
- Leahy, J. P., Bridle, A. H., & Strom R. G. 1998, Internet WWW page at URL: <<http://www.jb.man.ac.uk/atlas>>
- Lelièvre, G., & Wlérick, G. 1975, *A&A*, 42, 293
- Longair, M. S. 1994, *High Energy Astrophysics* (Cambridge Univ. Press, Cambridge)
- Lonsdale, C. J., Hartley-Davies, R., & Morison, I. 1983, *MNRAS*, 202, 1
- Marshall, H. L., Miller, B. P., Davis, D. S., et al. 2002, *ApJ*, 564, 683
- Meisenheimer, K., Yates, M. G., & Röser, H.-J. 1997, *A&A*, 325, 57
- Muraishi, H., Tanimori, T., Yanagita, S., et al. 2000, *A&A*, 54, L57
- Pesce, J. E., Sambruna, R. M., Tavecchio, F., et al. 2001, *ApJ*, 556, L79

- Röser, H.-J., Meisenheimer, M., Neumann, M., Conway, R. G., & Perley, R. A. 2000, *A&A*, 360, 99
- Sambruna, R. M., Urry, C. M., Tavecchio, F., et al. 2001, *ApJ*, 549, L161
- Saxton, C. J., Sutherland, R. S., Bicknell, G. V., et al. 2002, *A&A*, 393, 765
- Schwartz, D. A., Marshall, H. L., Lovell, J. E. J., et al. 2000, *ApJ*, 540, L69
- Stark, A. A., Gammie, C. F., Wilson, R. W., et al. 1992, *ApJS*, 79, 77
- Tanimori, T., Hayami, Y., Kamei, S., et al. 1998, *ApJ*, 497, L25
- Tavecchio, F., Maraschi, L., Sambruna, R. M., & Urry, C. M. 2000, *ApJ*, 544, L23
- Tregillis, I. L., Jones, T. W., & Ryu, D. 2001, *ApJ*, 557, 475
- Urry, C. M., & Padovani, P. 1995, *PASP*, 107, 803
- Wilson, A. S., Young, A. J., & Shopbell, P. L. 2000, *ApJ*, 544, L27
- Wilson, A. S., Young, A. J., & Shopbell, P. L. 2001, *ApJ*, 547, 740
- Wilson, A. S., & Yang, Y. 2002, *ApJ*, 568, 133